PHYSICAL REVIEW B **84**, 060101(R) (2011)

Imaging the dynamics of martensitic transitions using acoustic emission

Eduard Vives,[1,*] Daniel Soto-Parra,[2] Lluís Mañosa,[1] Ricardo Romero,[3] and Antoni Planes[1]
[1]*Departament d'Estructura i Constituents de la Matèria, Facultat de Física, Universitat de Barcelona, Diagonal, 647, E-08028 Barcelona, Catalonia, Spain*
[2]*Centro de Investigación en Materiales Avanzados S.C. Miguel de Cervantes 120, Complejo industrial Chihuahua, 31109 Chihuahua, México*
[3]*IFIMAT, Universidad del Centro de la Provincia de Buenos Aires and CICPBA, Pinto, 399, 7000 Tandil, Argentina*
(Received 18 July 2011; published 22 August 2011)

The acoustic emission associated with front propagation has been used to investigate the dynamics of a solid-solid martensitic phase transition. By using two sensors we have been able to locate the position of active fronts and to measure their associated energy release. The investigation of the reverse transitions occurring in a Cu-Zn-Al alloy from a stressed martensitic phase to a cubic phase at zero stress reveals significant differences in the front trajectories depending on whether the transition is driven by controlling the applied load (soft driving) or by controlling the elongation of the sample (hard driving). In agreement with theoretical predictions [F. J. Pérez-Reche, L. Truskinovsky, and G. Zanzotto, Phys. Rev. Lett. **99**, 075501 (2007)], we have observed different evolutions of the transition dynamics under cycling as well as other constrained kinetic effects.

DOI: 10.1103/PhysRevB.84.060101 PACS number(s): 81.30.Kf, 05.70.Jk, 43.40.Le, 64.60.av

Martensitic transitions (MTs) are known to be at the origin of a number of interesting functionalities such as shape memory and magnetic shape memory,[1] superelasticity,[2] and giant magnetomechanical caloric effects.[3–5] Understanding of the dynamics of these phase transitions has strong implications for the final control of their potential applications. In this Rapid Communication we present results based on the detection of acoustic emission (AE)[6] that allows a direct imaging of the MT dynamics in real space.

One of the aspects that makes martensitic alloys exceptional is the possibility of recovering from very large deformations ($\sim$10%) when an external force is applied. This occurs because, before reaching the elastic limit where irreversible plastic deformation should occur, the alloys undergo a structural change, typically from a cubic to a less symmetric phase. Among the symmetrically equivalent variants of the product phase, the system selects those that better adapt to the external applied stress. Although the elongation is fully recovered when the external force is released, the thermodynamic trajectories on the force versus elongation (F-X) diagram are not reversible, but display metastability and hysteresis phenomena. This is due to the existence of free-energy barriers much larger than thermal fluctuations, which originated from the interplay of elastic interactions and disorder.[7] Consequently, such systems do not reach full thermodynamic equilibrium, but remain trapped in metastable minima of a complex energy landscape. In such a situation the F-X trajectories depend not only on the history, but also on details of the driving mechanism.[8,9] For instance, such phase transitions can be driven by applying a controlled force that increases with time $F(t)$ (soft driving) or by controlling the elongation $X(t)$ at a constant rate (hard driving).

The understanding of the MT dynamics is strongly linked to the challenging problem of understanding the microscopic dynamics of a boundary separating two different crystallographic structures and its interaction with disorder.[10] For the particular case of athermal martensitic transitions (typically occurring at temperatures low enough so that thermal fluctuations can be neglected), fronts progress thanks to a local atomic rearrangement without long-range atomic diffusion. The advancement of an unstable front takes place at speeds similar to those of sound in the material, but it is interrupted due to pinning with defects and thermoelastic effects. Then it is necessary to maintain the action of a driving mechanism (cooling and heating, loading and unloading, etc.) in order to overcome the sequence of barriers separating metastable states. The fronts advance intermittently by avalanche dynamics.[11] This dynamics is acknowledged to be at the origin of the observed AE phenomenon: Acceleration of a front generates elastic waves (in the ultrasonic range 10^5–10^6 Hz) that propagate through the material and can be detected and studied by means of an appropriate transducer.[6]

Studies of energies associated with such AE events also reveal that avalanches have no characteristic scales and thus the MT front dynamics can be catalogued as being "critical."[12,13] Such a criticality associated with front propagation in disordered media is a long-standing problem in condensed-matter physics.[8] Several approaches have been proposed in order to provide an insight into this phenomenon. Recently it has been theoretically shown that, within the context of martensitic transitions, two types of criticality can be observed depending on the driving mechanism. If the transition is soft driven (controlling the applied force at a certain loading rate), one expects a process dominated by nucleation and, therefore, one should find critical properties typical of the so-called order-disorder (O-D) scenario. On the other hand, if one drives the transition by a *hard device* (controlling the deformation of the sample), one should observe a self-organized-criticality (SOC) type of critical point. The differences between the two cases should be revealed not only in the critical exponents, but also in the fact that within the first scenario one needs to tune the amount of disorder to reach criticality, whereas in the second scenario the constraint in length introduces an effective long-range force that forces the system to remain in the critical point, irrespective of the amount of disorder.[8]

The goal of this Rapid Communication is to investigate the dynamics of the active fronts during a MT under hard-driving and soft-driving conditions by means of an experimental technique based on the simultaneous detection of AE events

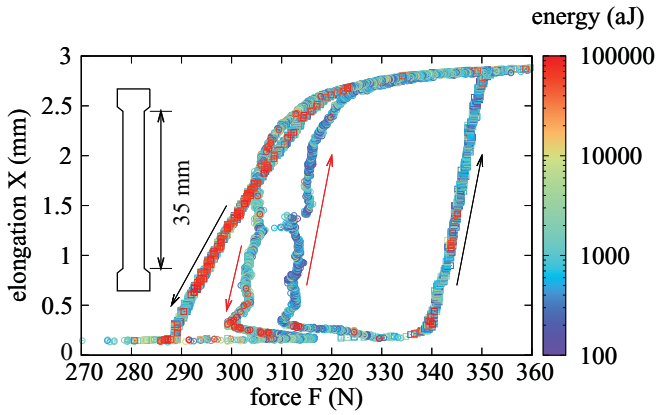

FIG. 1. (Color online) Comparison of the hysteresis loops obtained by imposing a constant elongation rate of 0.05 mm/min [hard-driving, red (gray) arrows] and a constant force rate of 0.31 N/s (soft driving, black arrows). The points indicate the values of the force and elongation measured synchronously with each detected AE event. The color indicates the source energy E_0 of the AE event. Data with energies larger than 5×10^4 aJ was plotted on top in order to facilitate localization of large acoustic events along the hysteresis loop.

by two transducers, which allows for the spatial location of the AE source.

We have studied a $Cu_{68.13}Zn_{15.74}Al_{16.13}$ single crystal grown by the Bridgman method. The sample has cylindrical heads and a 35 mm (long) × 1.4 mm × 3.95 mm body. The long direction (z) is oriented close to the [001] crystallographic direction. In the absence of applied external stress it exhibits a MT at $M_s = 234$ K from a cubic ($L2_1$) high-temperature parent phase to a monoclinic ($18R$) product phase. The transition can also be induced at room temperature by applying a uniaxial stress of ∼60 MPa. Prior to the sequence of studied load-unload cycles, an appropriate heat treatment was performed so that the sample was in the ordered state, free from internal stresses, and the vacancy concentration was minimum at room temperature. More sample details and heat treatments can be found elsewhere.[9,14] A schematic picture of the sample is shown in the inset of Fig. 1.

The two driving devices use the same sample grips, strain gauge, and load cell. The hard-driving machine is a commercial INSTRON 4302 that imposes a relative speed of the sample heads. The soft-driving machine, especially designed,[9] controls an increasing and decreasing dead load hanging from the sample.

Acoustic emission signals, as well as the readings from the strain gauge and load cell, are recorded by a PCI-2 acquisition system from Europhysical Acoustics. The simultaneous recording of the hits detected in two sensors (1 and 2),[15] placed close to the sample heads, allow localization of the AE source along the tensile z direction and the estimation of the energy E_0 of the source. We consider as true physical "events" only those which correspond to pairs of hits (one on each sensor) separated by a time difference $dt = t_1 - t_2$ less than $t_{max} = 0.038$ ms. This is the upper bound time interval for a signal to cross the full length ($L = 35$ mm) of the sample, and has been obtained from a previous calibration. This method enables the rejection of noise (electrical signals, signals coming from contact with the grips, or any other spurious phenomena occurring in the sample heads).

Let E_1 and E_2 be the energies detected by each sensor. Assuming a constant attenuation factor, we can obtain the vertical position z of the event and its source energy E_0 from the following expressions:[16]

$$z = \frac{1}{2}L\left(1 - \frac{dt}{t_{max}}\right), \quad E_0 = \sqrt{E_1 E_2}, \tag{1}$$

where constant prefactors in front of E_0 have been omitted. The validity of the expression for z has been crosschecked by using an external AE source on different positions on the sample both in the monoclinic (stressed) and cubic phases (unstressed). The uncertainty in z has been found to be less than ±0.35 mm. (Besides the resolution error, we have analyzed other sources of systematic errors such as the slightly different sound velocities in the two phases and the sample elongation. We have checked that these sources lead to distortions of the plots in Fig. 2 that are smaller than 5%.)

Figure 1 shows examples of the hysteresis loops obtained at room temperature with the two driving mechanisms. They reveal a ∼8% deformation under an applied stress of 65 MPa. The soft-driven loop (external) exhibits a larger hysteresis (which can be quantified as the area enclosed by the loading and unloading branches). The hard-driven loop (internal) exhibits a characteristic yield point where stress relaxation during loading occurs and strong stress fluctuations start.

Each data point in Fig. 1 corresponds to an AE event. The corresponding source energies E_0 (indicated by colors or gray tones) extend more than four orders of magnitude and have already been shown to be power-law distributed, as expected, for critical behavior.[17,18] The plot reveals some interesting features: There is more acoustic emission (higher density of points), and events are more energetic in the unloading branches as compared with the loading branches. The distribution of large events is clearly different when comparing the two driving mechanisms. In the soft-device case, large events are distributed more homogeneously along the phase transition path, whereas in the hard-device case, large events concentrate on the region where dX/dF is negative, after the yield point.

Starting from the state with minimum disorder, we have cyclically crossed the transition by loading and unloading at room temperature. As explained before we have located the position z of the source of each AE event in the vertical direction. Figure 2 shows the recorded positions as a function of time, as well as their energy (indicated by colors). We have focused on the analysis of the first four consecutive unloading branches after heat treatment and compared both a soft-driven (left-hand side) with a hard-driven experiment (right-hand side).

In all plots one can distinguish the existence of paths with a higher density of points (and also with more energetic events), which correspond to the trajectory of two main average fronts that move from the top ($z = 35$ mm) and bottom toward a point in the center of the sample. Once the two fronts meet, the transition ends and AE stops.

It is interesting to note that our acoustic technique reveals that the main propagating fronts display a certain internal structure. From optical imaging of the same sample[9] we know

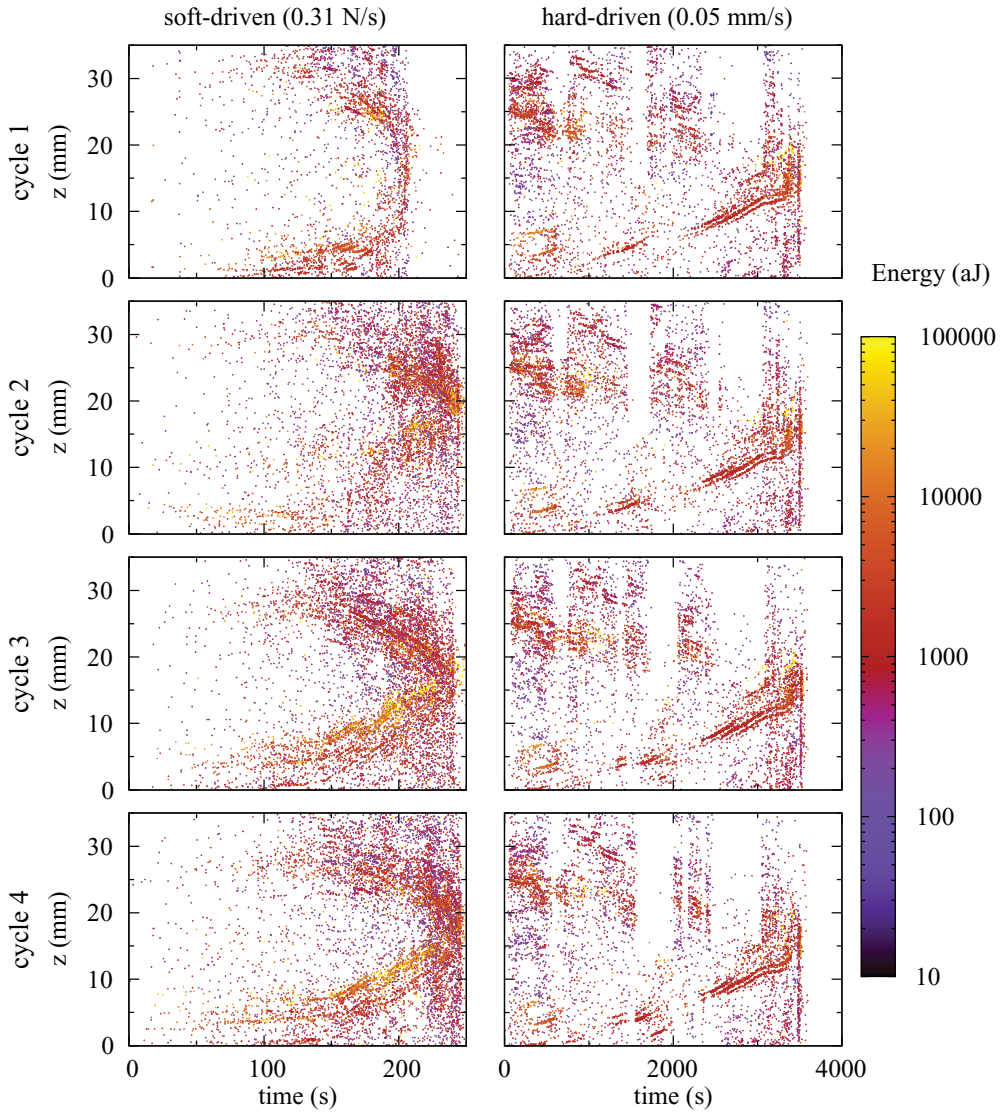

FIG. 2. (Color online) Vertical position of the AE source corresponding to each event as a function of time during the reverse martensitic transition. The different plots compare the evolution of the transition dynamics for the first four consecutive cycles after heat treatment, under soft-driving conditions (left-hand side) and hard-driving conditions (right-hand side).

that the transition takes place through the growth and shrinkage of thin parallel martensitic plates. The vector perpendicular to these plates forms an angle with the tensile axis which is consistent with the predictions of the phenomenological theory of martensites.[19] Figure 3 shows the magnification of the trajectory of one of these main fronts (corresponding to loop 3 in the hard-driven case), revealing that it is formed by a number of advancing sub-fronts that might correspond to individual domains growing simultaneously. The typical separation between the domains that are simultaneously active is $\sim$1 mm. Since the optical images found separations between plates ten times smaller,[14] this suggests that there are some dynamic interactions that allow only a few of the needle domains to advance simultaneously, giving rise to an AE footprint in our images. The effect is clearer in the hard-driven case, but also occurs in the soft-driven one.

Apart from the existence of the two main fronts, it is clear that small AE events occur all over the sample. For the soft-driven case, this extra activity mainly concentrates in the regions left behind the main fronts, compared with the regions that have not yet been crossed by the two fronts. In other words, there is a lot of AE activity associated with the retransformation of some regions, still in the martensitic phase, to the cubic phase.

For the hard-driven case another interesting feature can be directly observed: the existence of white vertical fringes, as well as the interruptions observed in the trajectories of the main fronts, indicating that when there is strong AE activity in the top front, there is no activity in the bottom one and vice versa. This confirms that the external constraint imposing a certain head velocity prevents both fronts from advancing simultaneously, whereas for the soft-driven case the two fronts can propagate simultaneously.

Concerning the dependence on cycling, for the soft-driven case there is a clear change when comparing the first loop (first retransformation) with the following ones. The first transition

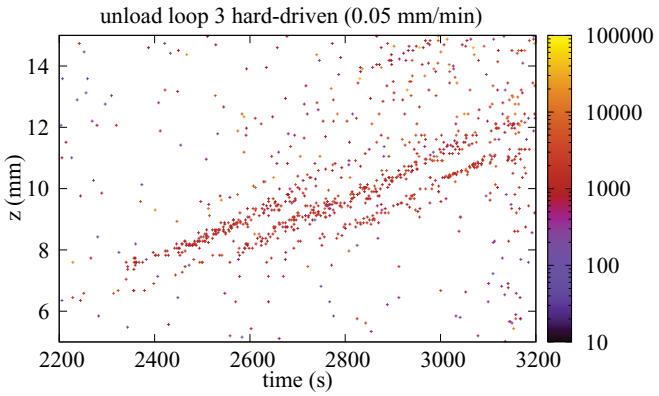

FIG. 3. (Color online) Detail of the third loop obtained by the hard-driving device, showing the evolution of simultaneous fronts with a separation of ∼1 mm.

is faster with much less AE activity. The trajectories of the main fronts have a parabolic shape, indicating an acceleration of the process, providing evidence that there are fewer pinning centres. In the second, third, and fourth loop the trajectories become more linear indicating a tendency to a constant velocity of the fronts and an increase in AE activity. Contrarily, for the hard-driven case almost no evolution with cycling is observed.

It is clear that the kinetics of the disorder in the sample is a crucial factor for a final understanding of the process. One should take into account not only the existence of quenched vacancies, dislocations, or impurities, but also, depending on the parent and product structures involved in the transition, the fact that the advancement of the interface itself creates or annihilates (nonquenched) structural defects such as dislocations. It has been shown[20] that during a cycling process through the martensitic transition the materials display the so-called "training" effect which has been explained as a consequence of this interaction between the transition fronts and the disorder created by the transition itself. Our results indicate that in the soft-driven case the system needs some initial cycling in order to tune the disorder and reach the critical state. For the hard-driven case the "training" effect is suppressed by the external constraint and the system is able to find a dynamical attractor with critical properties already from the first cycle. These results are in agreement both with the theoretical modeling[8] and previous analysis of the energy distribution of the AE signals.[21]

To conclude, we have shown that the simultaneous use of two AE transducers allows for direct imaging of the position of the fronts during structural transitions at a microscopic level. The experimental technique gives valuable kinetic information, complementary to optical microscopy. This method, applied to the case of a martensitic transition, has confirmed a number of theoretical hypotheses and has opened up questions that will definitely need further investigation. The most remarkable phenomena are those observed when the transition is driven by a hard device: (i) The main two transition fronts (moving from the top and the bottom) cannot advance simultaneously, (ii) big AE events concentrate in the trajectories with negative dX/dF after the yield stress, and (iii) martensite plates show dynamic interactions that prevent the simultaneous growth of those which are too close. Such conclusions could not be drawn from the analysis of static images.

This work has received financial support from the Spanish Ministry of Innovation and Science (project MAT2010-15114).

*eduard@ecm.ub.es

[1] See, for instance, *Science and Technology of Shape-Memory Alloys: New Developments*, Mater. Res. Soc. Bull. **27**, Issue 2 (2002).

[2] Y. Tanaka, Y. Himuro, R. Kainuma, Y. Sutou, T. Omori, and K. Ishida, Science **327**, 1488 (2010).

[3] T. Krenke, E. Duman, M. Acet, E. F. Wassermann, X. Moya, Lluis Mañosa, and A. Planes, Nat. Mater. **4**, 450 (2005).

[4] E. Bonnot, R. Romero, Ll. Mañosa, E. Vives, and A. Planes, Phys. Rev. Lett. **100**, 125901 (2008).

[5] Ll. Mañosa, D. González-Alonso, A. Planes, E. Bonnot, M. Barrio, J. Ll.Tamarit, S. Aksoy, and M. Acet, Nat. Mater. **9**, 478 (2010).

[6] C. B. Scruby, J. Phys. E **20**, 946 (1987).

[7] E. K. H. Salje, X. Ding, Z. Zhao, T. Lookman, and A. Saxena, Phys. Rev. B **83**, 104109 (2011).

[8] F. J. Pérez-Reche, L. Truskinovsky, and G. Zanzotto, Phys. Rev. Lett. **101**, 230601 (2008).

[9] E. Bonnot, R. Romero, X. Illa, Ll. Mañosa, A. Planes, and E. Vives, Phys. Rev. B **76**, 064105 (2007).

[10] T. Lookman, S. R. Shenoy, K. Ø. Rasmussen, A. Saxena, and A. R. Bishop, Phys. Rev. B **67**, 024114 (2003).

[11] F. J. Pérez-Reche, E. Vives, Ll. Mañosa, and A. Planes, Phys. Rev. Lett. **87**, 195701 (2001).

[12] E. Vives, J. Ortín, Ll. Mañosa, I. Ràfols, R. Pérez-Magrané, and A. Planes, Phys. Rev. Lett. **72**, 1694 (1994).

[13] R. Ahluwalia and G. Ananthakrishna, Phys. Rev. Lett. **86**, 4076 (2001).

[14] E. Bonnot, E. Vives, Ll. Mañosa, A. Planes, and R. Romero, Phys. Rev. B **78**, 094104 (2008).

[15] The technique can also be used to monitor other microscopic phenomena such as plastic flow. See J. Weiss and D. Marsan, Science **299**, 89 (2003).

[16] C. B. Scruby, K. A. Stacey, and G. R. Baldwin, J. Phys. D **19**, 1597 (1986).

[17] Ll. Carrillo, Ll. Mañosa, J. Ortín, A. Planes, and E. Vives, Phys. Rev. Lett. **81**, 1889 (1998).

[18] J. P. Sethna, K. A. Dahmen, and C. R. Myers, Nature (London) **410**, 242–250 (2001).

[19] C. M. Wayman, *Introduction to the Crystallography of Martensitic Transitions* (McMillan, New York, 1964).

[20] F. J. Pérez-Reche, L. Truskinovsky, and G. Zanzotto, Phys. Rev. Lett. **99**, 075501 (2007).

[21] E. Vives, D. Soto-Parra, Ll. Mañosa, R. Romero, and A. Planes, Phys. Rev. B **80**, 180101 (2009).